Decoupling of Rattling Mode and Superconductivity in Filled-Skutterudite $Ba_xIr_4Sb_{12}$

Hui Liu(刘辉)[1,2,3], Tongxu Yu(于同旭)[4], Zhihua Zhang(张志华)[1*], and Tianping Ying(应天平)[2,3*]

[1]*School of Materials Science and Engineering, Dalian Jiaotong University, Dalian 116028, China*
[2]*Institute of Physics, Chinese Academy of Sciences, Beijing 100190, China*
[3]*University of Chinese Academy of Sciences, Chinese Academy of Sciences, Beijing 100190, China*
[4]*Suzhou Laboratory, Suzhou 215123, China*

(Received 9 May 2024; accepted manuscript online 30 May 2024)

The rattling mode, an anharmonic vibrational phonon, is widely recognized as a critical factor in the emergence of superconductivity in caged materials. Here, we present a counterexample in a filled-skutterudite superconductor $Ba_xIr_4Sb_{12}$ ($x = 0.8$, 0.9, 1.0), synthesized via a high-pressure route. Transport measurements down to liquid ^{3}He temperatures reveal a transition temperature (T_c) of 1.2 K and an upper critical field (H_{c2}) of 1.3 T. Unlike other superconductors with caged structures, the $Ba_xIr_4X_{12}$ (X = P, As, Sb) family exhibits a monotonic decreasing T_c with the enhancement of the rattling mode, as indicated by fitting the Bloch–Grüneisen formula. Theoretical analysis suggests that electron doping from Ba transforms the direct bandgap $IrSb_3$ into a metal, with the Fermi surface dominated by the hybridization of Ir 5*d* and Sb 5*p* orbitals. Our findings of decoupled rattling modes and superconductivity distinguish the $Ba_xIr_4Sb_{12}$ family from other caged superconductors, warranting further exploration into the underlying mechanism.

DOI: 10.1088/0256-307X/41/7/077401

Numerous intriguing physical properties associated with caged structures, including exceptional thermal conductivity, exotic heat capacity, and superconductivity, are commonly attributed to the "rattling mode", i.e., an anharmonic vibrational mode originating from guest atoms located within the voids.[1–6] In the framework of the celebrating BCS theory, enhancing the rattling mode effectively strengthens electron–phonon coupling, potentially resulting in a higher transition temperature (T_c). A notable example is the β-pyrochlore oxide AOs_2O_6 (A = K, Rb, Cs). As the cation A radii increase from K to Rb and Cs, their transition temperatures T_c monotonically decrease from 9.6 K to 6.4 K and 3.25 K, respectively.[7–10] Evidently, the smaller K cation with more pronounced vibrational harmonicity contributes to the observed highest T_c. Theoretical calculations also support this rattling scenario, demonstrating that the atomic excursion of K along the body diagonal direction is significantly larger than those of its Rb and Cs counterparts.[11–14]

In addition to varying the radii of the guest cation, manipulating harmonicity can also be achieved by altering the size of the anions. As evidenced in skutterudite superconductors $LaRu_4P_{12}$ (T_c = 7.2 K) and $LaRu_4As_{12}$ (T_c = 10.4 K),[15–18] where the enlargement of the caged structure by replacing anion P for As effectively reduces the Debye temperature from 446 K to 355 K, and amplifies the rattling modes of the guest La, and consequently enhancing T_c.[16,17] Similar behavior is observed in intermetallic alloys, such as ScV_2Al_{20} and YV_2Al_{20}, reported as superconductors with T_c at 1.0 K and 0.6 K, respectively.[19,20] Further increasing the radii of rare earth elements leads to the quenching of superconductivity in LaV_2Al_{20},[21] consistent with this empirical rule. It is therefore widely accepted that strengthening of the rattling mode is a one-size-fits-all approach to enhancing desired properties in caged superconductors.[19,22,23]

Recent progress on $Ba_xIr_4X_{12}$ (X = P and As) raises doubts on this assertion. $Ba_xIr_4P_{12}$ and $Ba_xIr_4As_{12}$ are canonical skutterudite superconductors, where Ba fills the voids of semiconducting IrP_3 and $IrAs_3$, respectively, with the highest T_c at 5.6 K and 4.8 K, respectively.[24] Interestingly, substituting As for P creates a larger hollow space for the rattling Ba, yet the superconductivity in arsenide is inferior to that of phosphide. Additional clues arise from recent studies on hole-doped skutterudite compounds through a self-insertion process under high pressure, which gives T_c of 4.8 K and 4.4 K for P@IrP_3 and As@$IrAs_3$, respectively.[25] The similarity in T_c observed in both phosphides and arsenides, whether obtained through Ba-filled or self-inserted methods, undermines the conclusiveness of assessing the role of rattling modes in superconductivity. It is therefore highly desired to explore the antimonide, which should possess a larger cage and softer vibrational modes, offering potential insights into this phenomenon.

In this Letter, we report the successful growth of polycrystalline $Ba_xIr_4Sb_{12}$ (x = 0.8, 0.9, and 1.0) under high pressure. The acquired samples crystallize in the $Im\bar{3}$ space group (No. 204) and exhibit a significant increase in hollow voids, reaching 130% and 150% compared to those of its arsenide and phosphide counterparts, respectively.

*Corresponding authors. Email: zhzhang@djtu.edu.cn; ying@iphy.ac.cn
© 2024 Chinese Physical Society and IOP Publishing Ltd

A systematic decrease in the Debye temperature from P to As then to Sb indicates effective softening of the anharmonic vibrational modes of the guest Ba. Intriguingly, detailed transport measurements reveal a sharp resistance drop at 1.2 K in $Ba_{0.8}Ir_4Sb_{12}$, significantly lower than that of $Ba_{0.8}Ir_4As_{12}$ and $Ba_{0.8}Ir_4P_{12}$. These findings solidify our previous suspicions, suggesting that superconductivity in the $Ba_xIr_4Sb_{12}$ family may be decoupled from the rattling mode. Our results indicate that the variation in T_c found in skutterudites cannot be simply ascribed to a single explanation.

Experiments. Polycrystalline $Ba_xIr_4Sb_{12}$ was synthesized via high-pressure solid-state reactions, starting from pre-reacted $Ba_xIr_4Sb_{12}$ mixed with stoichiometric composition to 1173 K for 24 h. The pre-reacted raw material was thoroughly ground and placed in an h-BN capsule, then heated at 1673 K and 5 GPa for 4 h using a belt-type high-pressure apparatus. All starting materials and precursors were prepared in a glovebox filled with purified Ar gas (H_2O, $O_2 < 1$ ppm). It is worth noting that $Ba_xIr_4Sb_{12}$ is sensitive to the moisture and will deteriorate if exposed to air, necessitating storage in glovebox. Powder x-ray diffraction (XRD) patterns were obtained using a Bruker D8 Advance diffractometer with Cu K_α radiation at room temperature. Magnetization and transport properties were measured using a physical property measurement system (PPMS, Quantum Design). Low-temperature resistivity measurement was carried out using an Oxford Cryosystems setup with a ^{3}He insert. Density functional theory (DFT) calculations employed the projector augmented wave (PAW)[26] method implemented in the Vienna *ab initio* simulation package (VASP).[27] The PAW method describes wave functions near the core, and the generalized gradient approximation within the Perdew–Burke–Ernzerhof[28,29] parametrization is used as the electron exchange-correlation functional. Lattice constants and internal atomic positions were relaxed with a plane-wave cutoff energy of 600 eV, and forces were minimized to less than 0.01 eV/Å. The Monkhorst–Pack scheme[30] was used with a $5 \times 5 \times 5$ grid for structure relaxation and a $10 \times 10 \times 10$ grid for self-consistent calculations.

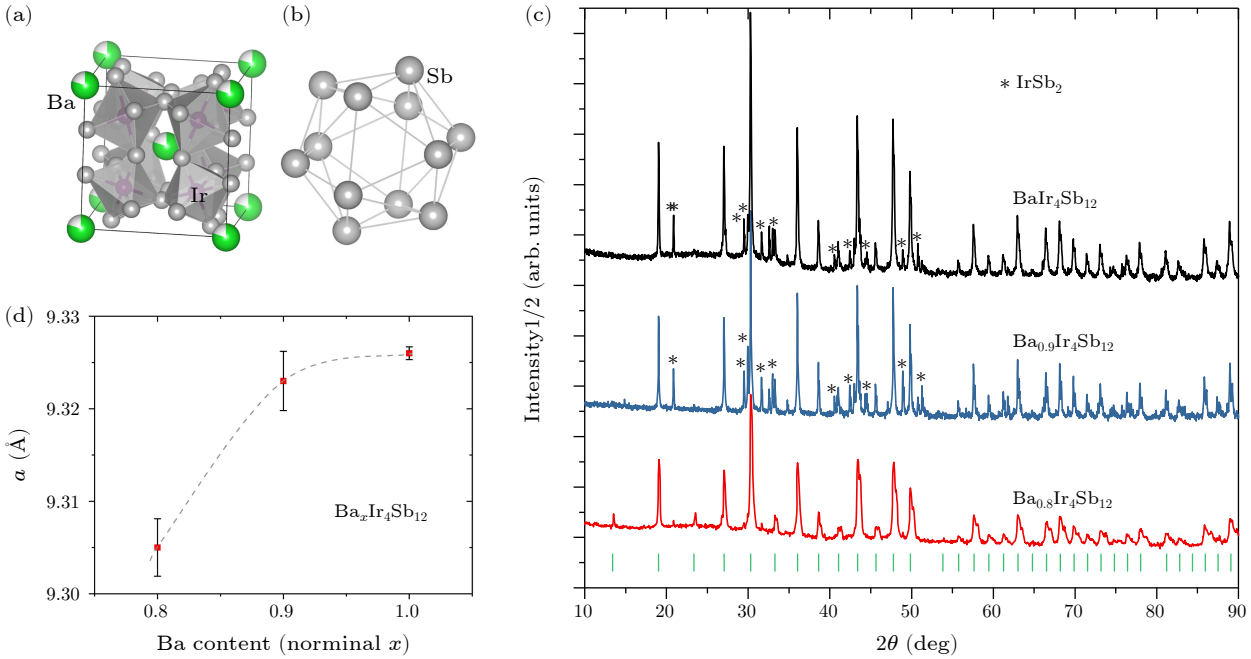

Fig. 1. Structure information of $Ba_xIr_4Sb_{12}$. (a) Crystal structure of $Ba_xIr_4Sb_{12}$. (b) The extracted 12 Sb anions are covalently connected to form a cage structure. (c) X-ray diffraction patterns of $Ba_xIr_4Sb_{12}$ with the nominal $x = 0.8$, 0.9, and 1. Stars denote the diffraction peaks arising from the $IrSb_2$ impurities. (d) The evolution of the a axis with the variation of Ba content, which slightly deviates from Vegard's law and tends to saturation with the increase of nominal doping content of Ba.

Results. Figure 1(a) illustrates the crystal structure of $Ba_xIr_4Sb_{12}$, featuring two cages (situated at the center and corner sites) constructed from twelve Sb anions [Fig. 1(b)]. Similar to its sister compounds, $Ba_xIr_4Sb_{12}$ can only be synthesized under high pressure of above 3 GPa. The x-ray diffraction (XRD) patterns of a series of Ba doping samples are shown in Fig. 1(c). The $Ba_{0.8}Ir_4Sb_{12}$ sample maintains the same cubic structure but with broadened peaks compared to $Ba_{0.8}Ir_4As_{12}$ and $Ba_{0.8}Ir_4P_{12}$. Further increasing the Ba content leads to the emergence of additional impurities such as $IrSb_2$, indicating a side reaction between Ba and $Ba_{0.8}Ir_4Sb_{12}$ at higher Ba content. The evolution of the a-axis versus the nominal composition is depicted in Fig. 1(d). The saturation tendency of the lattice parameter suggests that the highest Ba doping content lies between 0.8 and 0.9, similar to the highest filling ratio observed in $Ba_{0.85}Ir_4As_{12}$ and $Ba_{0.89}Ir_4P_{12}$ cases. It is noteworthy that replacing phosphide with antimony sig-

nificantly enlarges the lattice parameter from 8.1 (8.56) Å to 9.35 Å, resulting in an apparent expansion of the hollow space, which is 130% and 150% larger than that of $Ba_xIr_4As_{12}$ and $Ba_xIr_4P_{12}$, respectively.

The relatively broad diffraction peaks of the $x = 0.8$ sample, along with the gradually decreasing zero-field resistance curve, indeed raise concerns that the observed lower T_c may be influenced by disorder. Firstly, we noticed that the nominal $x = 0.9$ and $x = 1.0$ samples exhibit sharp diffraction peaks [as shown in Fig. 1(c)], despite the presence of an impurity phase, $IrSb_2$. Magnetization measurements of the nominal $x = 0.9$ and $x = 1.0$ samples down to 2 K showed no superconducting transition, indicating that the T_c's for these samples with sharp diffraction peaks are still much lower than those of their phosphide and arsenide counterparts. Secondly, through multiple peak fitting, such as for the 200 peak (Fig. S1 in the Supplementary Material), we observe that the diffraction peak can be split into two sets, corresponding to $a = 9.307$ Å and $a = 9.252$ Å, respectively. The latter matches perfectly to the lattice parameter of $IrSb_3$. Furthermore, through phase retrieval of the full diffraction pattern (Figs. S2 and S3 in the Supplementary Material), we confirm that all secondary peaks on the right side of the main diffractions originate from the unreacted $IrSb_3$. Therefore, the actual content of the intercalated Ba at 5 GPa should be located between 0.8 and 0.9, comparable to that of $Ba_{0.89}Ir_4P_{12}$ and $Ba_{0.85}Ir_4As_{12}$.[24]

The normal state temperature-dependent electrical resistivity of $Ba_{0.8}Ir_4Sb_{12}$ is depicted in Fig. 2(a). The sample exhibits metallic behavior from 2 K to 300 K, characterized by a broad hump feature around 70 K, and tends to saturate as it approaches room temperature. In a nonmagnetic metallic crystalline solid, resistivity can be elucidated within the framework of Boltzmann transport theory using the Bloch–Grüneisen formula

$$\rho(T) = \rho(0) + \rho_{\text{el-ph}}(T),$$

where $\rho(0)$ represents the residual resistivity caused by temperature-independent defect scattering. The temperature-dependent part of electron–phonon scattering, $\rho_{\text{el-ph}}(T)$, can be written as

$$\rho_{\text{el-ph}}(T) = \alpha_{\text{el-ph}} \left(\frac{T}{\Theta_R}\right)^n \int_0^{\Theta_R/T} \frac{x^n}{(e^x - 1)(1 - e^{-x})} dx,$$

where n takes the values of 2, 3, and 5, depending on the nature of electron–phonon interaction; $\alpha_{\text{el-ph}}$ is a constant proportional to the electron–phonon coupling constant, Θ_R is the Debye temperature. We superimposed the fitting results over the raw data shown by the black solid line in Fig. 2(a). The fitting demonstrates excellent agreement between the model and data, yielding $\alpha_{\text{el-ph}} = 0.020$, $\rho(0) = 0.0018$, $\rho_{\text{el-ph}}(T) = 5.512 \times 10^{-4}$. Additionally, a Debye temperature of 211 K was obtained, which is lower than that of $Ba_{0.85}Ir_4As_{12}$ at 311 K and $Ba_{0.89}Ir_4P_{12}$ at 368 K. This suggests the softening of vibrational modes in $Ba_{0.8}Ir_4Sb_{12}$. The realization of a metal-semiconductor transition in $IrSb_3$ through Ba doping, similar to Ba-doped IrP_3 and $IrAs_3$, prompted us to further investigate its low-temperature behavior. Figure 2(b) illustrates the resistivity down to 0.3 K, where a transition at 1.2 K becomes apparent. As the external magnetic field increases, the transition temperature gradually decreases, confirming the presence of superconductivity. Interestingly, the initial smooth downturn of the onset T_c becomes notably sharp at magnetic fields of $H = 0.25$ T and 0.5 T, different from the general observation of field suppression of superconductivity.[31–35] A plausible explanation is the presence of an inhomogeneous composition, where T_c of the acquired polycrystal ranges from 1.2 K to 0.8 K (judging from the onset T_c), while higher-trace superconductivity is quickly suppressed under a magnetic field, and the sharp transition at 0.8 K represents the bulk superconductivity of the acquired sample. Nevertheless, the realized T_c is only one fourth or one fifth of that of $Ba_{0.85}Ir_4As_{12}$ and $Ba_{0.89}Ir_4P_{12}$, unambiguously indicating a monotonic degradation of superconductivity with the enhancement of rattling modes.

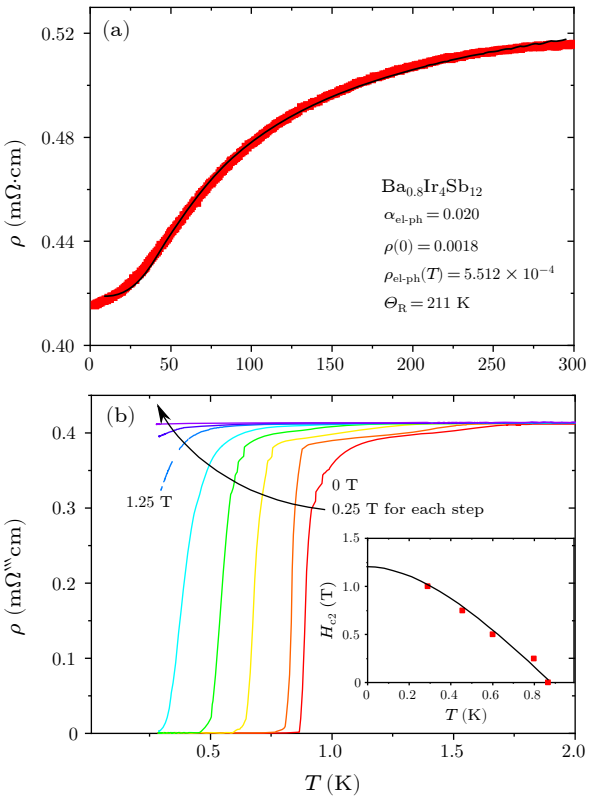

Fig. 2. Superconductivity in $Ba_xIr_4Sb_{12}$. (a) Temperature-dependent resistivity of $Ba_{0.8}Ir_4Sb_{12}$ from 2 K to 300 K. (b) Resistivity of $Ba_{0.8}Ir_4Sb_{12}$ down to 0.3 K under various magnetic fields. Inset is the upper critical magnetic field extracted from (b). The broken curve represents the Ginzburg–Landau fitting, yielding $H_{c2} = 2$ T.

The upper critical fields (H_{c2}) of the $Ba_xIr_4Sb_{12}$ family exhibit irregular evolution. Above $H = 1$ T, the sharp transition gradually smears out, and at $H = 2$ T, the superconducting transition cannot be observed above 0.3 K. The T_c's for each magnetic field are extracted and plotted

in Fig. 2(b) and the H_{c2} is fitted using Ginzburg–Landau formula[36,37]

$$\mu_0 H_{c2}(T) = \mu_0 H_{c2}(0)(1-t^2)/(1+t^2),$$

where the parameter $t = T/T_c$ is the reduced temperature with zero-field superconducting T_c. By the above fitting we obtain an upper critical magnetic field (H_{c2}) of 2 T, consistent with the expected value of the Pauli limit ($B_{\mathrm{Pauli}}(T) = 1.84\,\mathrm{T\cdot K^{-1}}\,T_c$) and close to that of $Ba_{0.89}Ir_4P_{12}$ ($H_{c2} = 2.9$ T), but much lower than that of $Ba_{0.85}Ir_4As_{12}$ ($H_{c2} = 6.9$ T). The superconductivity in $Ba_xIr_4Sb_{12}$ falls within the realm of weakly correlated BCS framework.

The band structures of raw $IrSb_3$ and $Ba_xIr_4Sb_{12}$ with spin–orbit coupling (SOC) are depicted in Figs. 3(a) and 3(b), respectively. Different from the indirect band gap in IrP_3, $IrSb_3$ resembles $IrAs_3$ and shows a zero direct band gap at Γ point. Due to the metallicity of antimony, $IrSb_3$ behaves as a semimetal and its resistivity at low temperatures is several orders of magnitudes lower than those of $IrAs_3$ and IrP_3. Upon Ba filling, $Ba_xIr_4Sb_{12}$ can be viewed as undergoing a rigid band shift by populating the conduction bands. In Fig. 3(c), it is evident that the Fermi level is primarily dominated by the d orbitals of Ir and p orbitals of Sb. The hybridization of d–p orbitals at the Fermi level is responsible for the conductivity observed in the acquired sample.

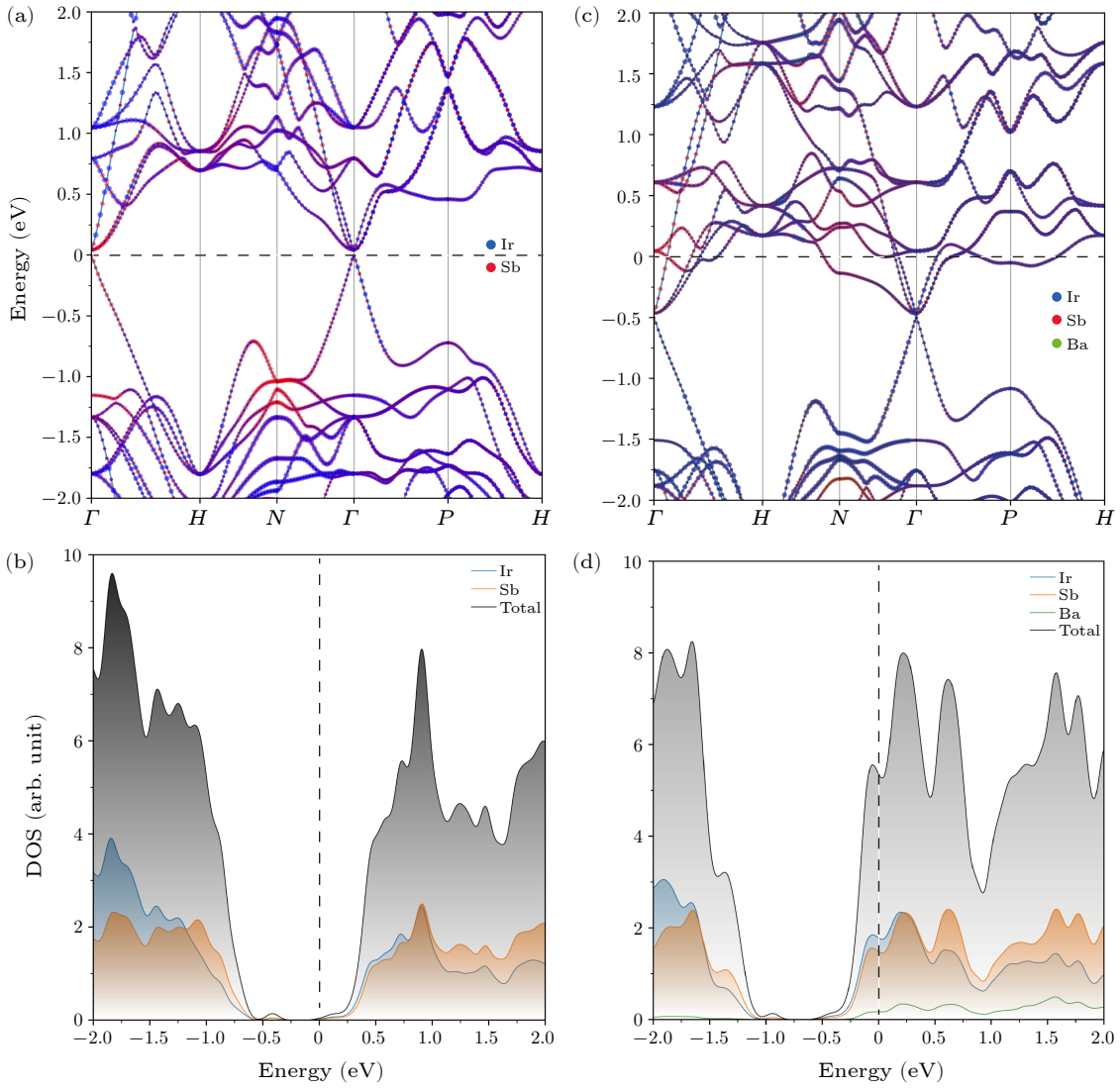

Fig. 3. Band structures and density of state (DOS) of $IrSb_3$ [(a), (b)] and $Ba_xIr_4Sb_{12}$ [(c), (d)].

The monotonic evolution of T_c in both Ba-filled and high-pressure samples from P through As to Sb prompts us to investigate the primary factor driving the emergence of superconductivity. We initially examine the influence of electron doping. Since the samples prepared in this study with $x > 0.8$ contain $IrSb_2$ as an impurity, the nominal compositions of $x = 0.9$ and 1.0 should be deficient but still higher than 0.8, considering the slight lattice expansion shown in Fig. 1(d). Upon revisiting our previous results, we make an interesting discovery: the T_c's of $Ba_{0.8}Ir_4As_{12}$

and $Ba_{0.8}Ir_4P_{12}$ are nearly identical at 4.5 K (the slope of dT_c/dx for $Ba_xIr_4P_{12}$ differs from that of $Ba_xIr_4As_{12}$, yielding an exact value of 4.43 K for $Ba_{0.8}Ir_4P_{12}$). As shown in Fig. 3(b), the spectral weight of Ba is negligible near the Fermi level, indicating that Ba has donated all its outer-shell electrons to Ir and Sb, leaving its empty s orbit high above the Fermi level (E_F). With an equivalent counting of valence electrons, the observed superconductivity in the filled IrX_3 (X = P, As, and Sb) must have an alternative origin other than electron doping.

For the same reason, the similar T_c observed in $Ba_{0.8}Ir_4As_{12}$ and $Ba_{0.8}Ir_4P_{12}$ rule out the possibility of chemical pressure. Furthermore, chemical pressure is unlikely to influence the caged atoms as they are generally far detached from the lattice. It has been suggested that the softening of phonon modes is responsible for the T_c enhancement in $LaRu_4P_{12}$ ($T_c = 7.2$ K and $\Theta_D = 566$ K) and $LaRu_4As_{12}$ ($T_c = 10.4$ K and $\Theta_D = 383$ K). However, this explanation does not hold true here, as the average Debye temperature of $Ba_xIr_4Sb_{12}$ (211 K) is much lower than that of $Ba_xIr_4As_{12}$ (311 K) and $Ba_xIr_4P_{12}$ (368 K), yet the T_c in the Sb compound is significantly lower than those in the As and P compounds. We can therefore exclude possibility of the strengthening of low-frequency anharmonic vibrational modes for the observed superconductivity in the $Ba_{0.8}Ir_4Sb_{12}$ family.

A wealth of research has focused on the induction or enhancement of superconductivity through rattling modes, primarily driven by strong electron-rattler interactions. This phenomenon is exemplified in various materials, including β-pyrochlore oxides,[21] Ge/Si clathrates,[38] and filled skutterudites.[39] In these systems, guest atoms residing within large spheres weakly connect to the cage structure, enabling significant excursions in quasi-quartic potential and contributing to anharmonic vibrational modes. As rattling strength increases, a transition from weak to strong coupling is often observed, as seen in the evolution from $CsOs_2O_6$ to KOs_2O_6.[40] While many caged structures adhere to this pattern, exceptions such as $LaRu_4X_{12}$ and $LaOs_4X_{12}$ challenge this tendency by exhibiting increasing T_c from P to As, but decreasing for the Sb case.[41,42] These anomalies suggest the need to consider additional factors, such as multiband structure and spin-orbital coupling (SOC). Notably, our discovery of superconducting $Ba_{0.8}Ir_4Sb_{12}$ distinguishes this family as the sole example showing a monotonic decline in T_c among all caged superconductors.

Taking into account the considerations mentioned above, we propose two plausible explanations to qualitatively elucidate the observed phenomena. Firstly, it is well established that the strength of SOC is proportional to Z^4, where Z represents the atomic number of the element. It has been demonstrated that an increase in SOC can lead to a decrease in electron–phonon interaction, and consequently, a reduction in T_c. Prominent examples are the Li_2Pd_3B ($T_c = 8$ K) and Li_2Pt_3B ($T_c = 2.8$ K),[43] where the enhancement of SOC not only leads to the decreased T_c, but also the alteration of the electron pairing mechanism from spin singlet to spin triplet. Similar phenomena have also been observed in Y_2C_3 ($T_c = 18$ K) and La_2C_3 ($T_c = 13$ K).[44,45]

Secondly, within the framework of BCS theory, Cooper pairs can be coupled by either acoustic or optical phonons. The rattling phonon affects superconductivity through its interaction with lattice vibrations and the renormalization of the phonon dispersion and the electron–phonon coupling constant. The heavier cage elements will result in low-lying acoustic phonon branches below the rattling phonon modes.[46,47] Therefore, if the electron coupling in the $Ba_xIr_4X_{12}$ family is facilitated by acoustic phonons, substituting the cage element from P to As and to Sb will naturally diminish the contribution of the rattling phonon. This may also explain our observed decoupling of the rattling mode and superconductivity. We anticipate further investigation to yield a deeper understanding of the unique T_c evolution in these caged superconductors.

In conclusion, we have successfully induced superconductivity in $IrSb_3$ by Ba doping. X-ray diffraction analysis reveals that $Ba_xIr_4Sb_{12}$ shares an isostructural relationship with its $Ba_xIr_4P_{12}$ and $Ba_xIr_4As_{12}$ counterparts and the maximum filling rate of Ba is 80% under 5 GPa. Transport measurements down to 0.3 K unveil a T_c of 1.2 K for $Ba_{0.8}Ir_4Sb_{12}$ and H_{c2} of 2 T. Notably, $Ba_xIr_4X_{12}$ (X = P, As, and Sb) is the first family in caged superconductors that shows a monotonic decreasing T_c with the strengthening of anharmonic vibrations of the guests. Through theoretical calculations and comparison with other systems, we conclude that the evolution of superconductivity in the IrX_3 (X = P, As, and Sb) family cannot solely be attributed to the phonon-softening mechanism. These findings prompt further systematic exploration of the skutterudite family to unravel the intricate superconductivity mechanisms within these multifarious caged structures.

Acknowledgments. This work was supported by Beijing Natural Science Foundation (Grant No. Z200005), the National Key Research and Development Program of China (Grant No. 2021YFA1401800), and the National Natural Science Foundation of China (Grant Nos. 52272267 and 52202342).

References

[1] Xiong C, Pei C Y, Wang Q, Wu J F, Zhao Y, Jiang Y Y, Li C H, Cao W Z, Yu N, Zhang L L, and Qi Y P 2024 *Phys. Rev. B* **109** 075202

[2] Bhattacharyya A, Adroja D T, Jana A K, Panda K, Ferreira P P, Zhao Y, Ying T, Hosono H, Dorini T T, Eleno L T F, Biswas P K, Stenning G, Tripathi R, and Qi Y 2024 *J. Alloys Compd.* **978** 173374

[3] Hong A and Ma L 2021 *Appl. Phys. Lett.* **118** 143903

[4] Lingannan G, Joseph B, Sundaramoorthy M, Kuo C N, Lue C S, and Arumugam S 2022 *J. Phys.: Condens. Matter* **34** 245601

[5] Sluchanko N, Bogach A, Bolotina N, Glushkov V, Demishev S, Dudka A, Krasnorussky V, Khrykina O, Krasikov K, Mironov V, Filipov V B, and Shitsevalova N 2018 *Phys. Rev. B* **97** 035150

[6] Pei C Y, Ying T P, Zhao Y, Gao L L, Cao W Z, Li C H, Hosono H, and Qi Y P 2022 *Matter Radiat.* **7** 038404

[7] Hiroi Z, Yonezawa S, Muramatsu T, Yamaura J I, and Muraoka Y 2005 *J. Phys. Soc. Jpn.* **74** 1255

[8] Yamaura J I, Yonezawa S, Muraoka Y, and Hiroi Z 2006 *J. Solid State Chem.* **179** 336

[9] Nagao Y, Yamaura J I, Ogusu H, Okamoto Y, and Hiroi Z 2009 *J. Phys. Soc. Jpn.* **78** 064702

[10] Lee C C, Lee W L, Lin J Y, Tsuei C C, Lin J G, and Chou F C 2011 *Phys. Rev. B* **83** 104503

[11] Hiroi Z, Yonezawa S, Nagao Y, and Yamaura J 2007 *Phys. Rev. B* **76** 014523

[12] Hattori K and Tsunetsugu H 2010 *Phys. Rev. B* **81** 134503

[13] Oshiba K and Hotta T 2011 *J. Phys. Soc. Jpn.* **80** 094712

[14] Hattori K and Tsunetsugu H 2009 *J. Phys. Soc. Jpn.* **78** 013603

[15] Bochenek L, Wawryk R, Henkie Z, and Cichorek T 2012 *Phys. Rev. B* **86** 060511

[16] Uchiumi T, Shirotani I, Sekine C, Todo S, Yagi T, Nakazawa Y, and Kanoda K 1999 *J. Phys. Chem. Solids* **60** 689

[17] Tütüncü H M, Karaca E, and Srivastava G P 2017 *Phys. Rev. B* **95** 214514

[18] Klotz J, Götze K, Lorenz V, Prots Y, Rosner H, Harima H, Bochenek L, Henkie Z, Cichorek T, Sheikin I, and Wosnitza J 2019 *Phys. Rev. B* **100** 205106

[19] Winiarski M J, Wiendlocha B, Sternik M, Wiśniewski P, O'Brien J R, Kaczorowski D, and Klimczuk T 2016 *Phys. Rev. B* **93** 134507

[20] Koza M M, Leithe-Jasper A, Sischka E, Schnelle W, Borrmann H, Mutka H, and Grin Y 2014 *Phys. Chem. Chem. Phys.* **16** 27119

[21] Hiroi Z, Yamaura J I, and Hattori K 2012 *J. Phys. Soc. Jpn.* **81** 011012

[22] Hiroi Z, Onosaka A, Okamoto Y, Yamaura J I, and Harima H 2012 *J. Phys. Soc. Jpn.* **81** 124707

[23] Nemoto Y, Yanagisawa T, Yasumoto Y, Kobayashi H, Yamaguchi A, Tsuduku S, Goto T, Takeda N, Ochiai A, Sugawara H, Sato H, and Kitazawa H 2008 *J. Phys. Soc. Jpn.* **77** 153

[24] Qi Y P, Lei H C, Guo J G, Shi W J, Yan B H, Felser C, and Hosono H 2017 *J. Am. Chem. Soc.* **139** 8106

[25] Pei C Y, Ying T P, Zhang Q H, Wu X X, Yu T X, Zhao Y, Gao L L, Li C H, Cao W Z, Zhang Q, Schnyder A P, Gu L, Chen X L, Hosono H, and Qi Y P 2022 *J. Am. Chem. Soc.* **144** 6208

[26] Blöchl P E 1994 *Phys. Rev. B* **50** 17953

[27] Kresse G and Furthmüller J 1996 *Phys. Rev. B* **54** 11169

[28] Perdew J P, Burke K, and Ernzerhof M 1996 *Phys. Rev. Lett.* **77** 3865

[29] Ernzerhof M and Scuseria G E 1999 *J. Chem. Phys.* **110** 5029

[30] Monkhorst H J and Pack J D 1976 *Phys. Rev. B* **13** 5188

[31] Chen X, Deng J, Jin S F, Ying T P, Fei G, Ren H F, Yang Y F, Ma K, Yang M Z, Wang J J, Li Y C, Chen X, Liu X B, Du S X, Guo J G, and Chen X L 2023 *J. Am. Chem. Soc.* **145** 17435

[32] Chen X, Zhang X, Xiao X, Wang Z J, and Zhao J Z 2023 *Angew. Chem. Int. Ed.* **62** e202216010

[33] Ying T P, Wang M X, Wu X X, Zhao Z Y, Zhang Z Z, Song B Q, Li Y C, Lei B, Li Q, Yu Y, Cheng E J, An Z H, Zhang Y, Jia X Y, Yang W, Chen X H, and Li S Y 2018 *Phys. Rev. Lett.* **121** 207003

[34] Ying T P, Chen X L, Wang G, Jin S F, Zhou T T, Lai X F, Zhang H, and Wang W Y 2012 *Sci. Rep.* **2** 426

[35] Chen X, Zhan X H, Wang X J, Deng J, Liu X B, Chen X, Guo J G, and Chen X L 2021 *Chin. Phys. Lett.* **38** 057402

[36] Askerzade I N 2006 *Phys. Usp.* **49** 1003

[37] Stephen M J 1965 *Phys. Rev.* **139** A197

[38] Myles C W, Biswas K, and Nenghabi E 2007 *Physica B* **401–402** 695

[39] Cao D, Bridges F, Chesler P, Bushart S, Bauer E D, and Maple M B 2004 *Phys. Rev. B* **70** 094109

[40] Hinokihara T and Miyake K 2012 *J. Phys. Soc. Jpn.* **81** 084603

[41] Shirotani I, Uchiumi T, Ohno K, Sekine C, Nakazawa Y, Kanoda K, Todo S, and Yagi T 1997 *Phys. Rev. B* **56** 7866

[42] Shirotani I, Ohno K, Sekine C, Yagi T, Kawakami T, Nakanishi T, Takahashi H, Tang J, Matsushita A, and Matsumoto T 2000 *Phys. Rev. B* **281–282** 1021

[43] Yuan H, Vandervelde D, Salamon M, Badica P, and Togano K 2006 *AIP Conf. Proc.* **850** 633

[44] Smidman M, Salamon M B, Yuan H Q, and Agterberg D F 2017 *Rep. Prog. Phys.* **80** 036501

[45] Muranaka T and Akimitsu J 2016 *Chem. Sci. J.* **7** 1000135

[46] Wu J Z, Akagi K, Xu J T, Shimotani H, Huynh K K, and Tanigaki K 2016 *Phys. Rev. B* **93** 094303

[47] Wu J Z, Xu J T, and Tanigaki K 2024 *J. Phys. Chem. Solids* **184** 111709